ACS OMEGA
Article
Cite This: ACS Omega 2018, 3, 1663−1674

Interfacial Behavior of Cs^+, K^+, Na^+, and Rb^+ Extraction in the Presence of Dibenzo-18-Crown-6 from the Nitrobenzene−Water Biphasic System: Experimental, Quantum Chemical, and Molecular Dynamic Studies

Rima Biswas,[†] Pallab Ghosh,[†] Tamal Banerjee,[*,†] Sk. Musharaf Ali,[‡] and Ashish Kumar Singha Deb[‡]

[†]Department of Chemical Engineering, Indian Institute of Technology Guwahati, Guwahati, 781039 Assam, India
[‡]Bhabha Atomic Research Center, Chemical Engineering Division, Mumbai, 400085 Maharashtra, India

Supporting Information

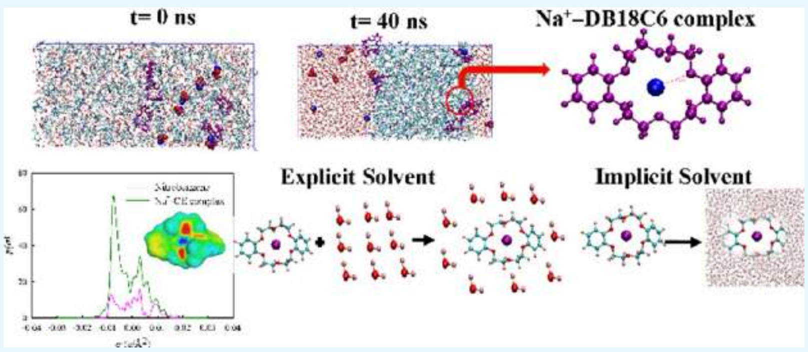

ABSTRACT: Extraction of metal ions (i.e., Cs^+, K^+, Na^+, and Rb^+) in the presence of ionophore such as dibenzo-18-crown-6 (DB18C6) from the nitrobenzene−water biphasic system is reported by COSMO-RS (conductor-like screening model for real solvents) predictions, molecular dynamics simulation, along with experimental validation. The predicted values of selectivity as obtained for the Na^+−DB18C6 complex were 4.571, 4.877, and 4.947 at 298.15, 308.15, and 318.15 K, respectively. This was then confirmed by the experimental distribution coefficient (D) as obtained in the diluent systems along with by varying the metal ion to crown ether ligand (M−L) mole ratios: 10:1 (0.1 M M^+ and 0.01 M DB18C6), 1:1 (0.01 M M^+ and 0.01 M DB18C6), and 1:10 (0.001 M M^+ and 0.01 M DB18C6). The experimentally determined values of D_{Na} (i.e., 0.059, 0.060, and 0.056) were found to be very large as compared to the values of D_{Cs} (i.e., 0.001, 0.010, and 0.024) in the nitrobenzene phase. It indicates an excellent extraction ability of DB18C6 for Na^+. The rate of phase separation for the $Cs^+NO_3^-$ system was slow as compared to other metal ion systems. The binding energies, free energies, and nonbonded interaction energies of the complexed metal ion in solution were calculated with both explicit and implicit solvent models. A higher interaction energy between Na^+−DB18C6 complex and nitrobenzene was observed (i.e., −289.92 in the explicit model and −143.12 kcal/mol in the implicit model) when compared with other metal ions (i.e., Cs^+, K^+, and Rb^+).

1. INTRODUCTION

Extraction of metal ions is considered to be a very complex process. The spent nuclear fuel contains a small amount of ^{137}Cs and a large amount of Na^+, which is a major heat-generating radionuclide.[1,2] Removal of radionuclide leads to reduction in heat load, which lowers the volume of repository required for final vitrification. The partitioning of these radionuclides is one of the most difficult challenges in spent nuclear reprocessing. Specific ionophores such as calix[4]arene-crown-6 ethers are extensively used for the extraction of cesium ion from the nuclear waste solution.[3] Removal of cesium ion using crown ether (CE) has been reported earlier by Luo et al.[4] and McDowell et al.[5] The application of CE has been found to be very efficient for the extraction of metal ions such as cesium, sodium, and potassium.[4]

Along with the ionophore, the diluent also plays a major role in liquid−liquid extraction. The ionophore is usually soluble in the diluent, which aids in the metal ion coordination. The use of nitrobenzene as an organic diluent for the extraction of alkali metal ions using dibenzo-18-crown-6 (DB18C6) has been reported by Makrlík et al.[6] Michael et al.[7] reported a theoretical study on the neat water−nitrobenzene liquid−liquid interface at 300 K. Jorge et al.[8] further studied the intrinsic structure and dynamics of the water−nitrobenzene interface. Continuing with the same trend, the transfer of calcium ion across the water−

Received: November 21, 2017
Accepted: January 29, 2018
Published: February 8, 2018

nitrobenzene interface has also been performed by Santos et al.[9]

On the basis of this perspective, a need is felt for a comprehensive study involving the two-phase system, that is, the CE and the metal ion. One of the commonly used quantum chemical (QC)-based models, that is, COSMO-RS (conductor-like screening model for real solvents),[10] is based on the integration of QC calculations and a statistical mechanical framework. This model is used to determine the activity coefficient of any component in the system by placing the solute in the midst of a conductor, so as to attain perfect screening. The screening charges developed are used to predict the chemical potential and the activity coefficient.[11,12] However, COSMO-RS predicts equilibrium properties and hence may not provide a deep understanding of the solvation and transport mechanism. To get a wide picture, molecular dynamic (MD) simulations are necessary. Although COSMO-RS will help us in predicting the Gibbs solvation free energy, MD will provide information on the demixing index (rate of phase separation) and radial distribution functions (RDFs).

We have also attempted to predict the interaction energies during complexation for the metal ion−ionophore pair using density functional theory (DFT) optimizations within a polarizable continuum model (PCM) and an explicit solvent model. Together, we shall be able to obtain lucid information on the underlying mechanism of charge transfer.

2. RESULTS AND DISCUSSION

2.1. COSMO-RS Predictions. Within the COSMO-RS mode, the sigma profile is a useful descriptor which defines the polarity of two adjacent molecules or segments. These are depicted in Figure 1, indicating the local polarity of the molecular surfaces. The hydrogen-bonding cutoff region for screening charge density (σ) is defined by the hydrogen bond acceptor ($\sigma_{HB} < -0.0084$ e/Å^2) and hydrogen bond donor ($\sigma_{HB} < +0.0084$ e/Å^2).[13] A fraction of sigma profile in the acceptor region ($\sigma_{HB} < -0.0084$ e/Å^2) defines the electropositive charge of the molecule, which shows the ability of the respective section to donate a hydrogen bond. This is evident from the sharp peak of the metal ion, which is positive in nature. The screening charges developed are opposite to that of the inherent solute density. On the other hand, a fraction of the sigma profile in the donor region ($\sigma_{HB} > +0.0084$ e/Å^2) defines an electronegative part of the molecule, which indicates its ability to accept a hydrogen bond. This corresponds to the anion of the metal salts. The sigma profiles of DB18C6 along with the metal ion (or the complexes) are shown in Figure 1a. From the sigma profiles, it is implied that the metal ions (Figure 1b) are located toward the hydrogen bond donor region, that is, σ_{HB}, or the cutoff for hydrogen bond energy is greater than +0.0084 e/Å^2. A contrary is observed for the metal ion complex where the majority of the profile lies in the nonpolar region of -0.0084 e/Å^2 < σ_{HB} < +0.0084 e/Å^2. This indicates that after the capture, it indeed becomes hydrophobic and tends to have a potential to diffuse into another solvent. This indicates an increased stability of the metal ions when encompassed within the ionophore.

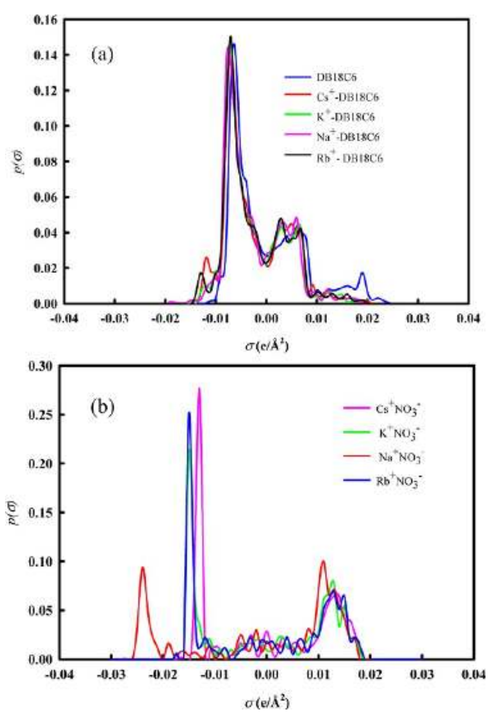

Figure 1. Sigma Profiles of (a) DB18C6 (blue), Cs^+−DB18C6 (red), K^+−DB18C6 (green), Na^+−DB18C6 (pink), and Rb^+−DB18C6 (black) and (b) $Cs^+NO_3^-$ (pink), $K^+NO_3^-$ (green), $Na^+NO_3^-$ (red), and $Rb^+NO_3^-$ (blue).

The screening charge density of DB18C6 and its complexes is shown in Figure 2a−e. The red portion shows the positive surface screening charge within the CE cavity, whereas the blue region corresponds to the negative surface charge of the trapped metal ion (Figure 2b−e). It is interesting to observe that the charge neutralization on the introduction of metal ion is highly dispersed in the case of Cs^+ extraction (Figure 2b) when compared to the same for Na^+ (Figure 2d). However, we cannot comment on the nature of interaction or binding energies because we do not know the absolute activity coefficient. This can be decided by the selectivity values which are experimentally observed.

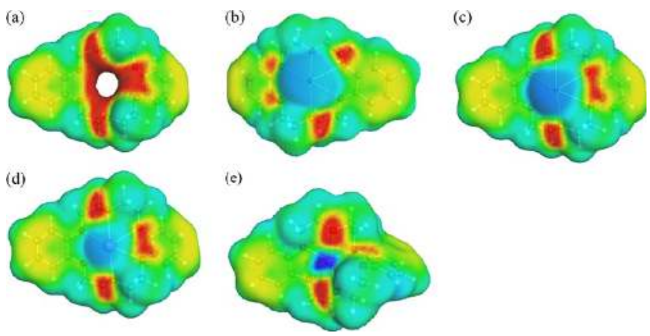

Figure 2. COSMO segmented surface of (a) DB18C6, (b) Cs^+−DB18C6 complex, (c) Rb^+−DB18C6 complex, (d) K^+−DB18C6 complex, and (e) Na^+−DB18C6 complex.

The selectivities for the metal ions and their complexes in the nitrobenzene−water binary system at three temperatures (i.e., 298.15, 308.15, and 318.15 K) are listed in Table 1. The selectivity (S) of the solutes was obtained from the ratio of the aqueous species in the nitrobenzene-rich phase (extract) to the complex in the nitrobenzene-rich phase.[14]

$$S_{12}^{\infty} = \left(\frac{\gamma_2^{\infty}}{\gamma_1^{\infty}}\right)^{\text{nitrobenzene}} \left(\frac{\gamma_1^{\infty}}{\gamma_2^{\infty}}\right)^{\text{water}} \approx \left(\frac{\gamma_2^{\infty}}{\gamma_1^{\infty}}\right)^{\text{nitrobenzene}} \tag{1}$$

DOI: 10.1021/acsomega.7b01828
ACS Omega 2018, 3, 1663−1674

Table 1. COSMO-RS-Predicted Selectivities of Solutes in Nitrobenzene−Water Systems at Different Temperatures

solutes	298.15 K	308.15 K	318.15 K
$Cs^+NO_3^-$	0.348	0.354	0.361
$Rb^+NO_3^-$	0.362	0.364	0.366
$K^+NO_3^-$	0.406	0.409	0.412
$Na^+NO_3^-$	1.285	1.257	1.231
Cs^+−CE complex	1.607	1.651	1.697
Rb^+−CE complex	1.651	1.711	1.755
K^+−CE complex	3.562	3.760	3.994
Na^+−CE complex	4.571	4.877	4.947

where γ_1^∞ and γ_2^∞ are the activity coefficients of the complex and water at infinite dilution. The selectivity of metal ions is found to be lower than that of the complexed metal ions in the nitrobenzene−water binary system. For the calculation, we have assumed a complete dissociation of the metal salts. Thus, the sigma profiles of the individual ions are linearly added up as per their individual sigma profile.[14] The selectivity was found to decrease with increasing metal ion size, that is, $Na^+ > K^+ > Rb^+ > Cs^+$. The selectivities of $Na^+NO_3^-$ (i.e., 1.285, 1.257, and 1.231) were found to be higher than those of other metal ions, that is, $K^+NO_3^-$, $Rb^+NO_3^-$, and $Cs^+NO_3^-$. Similarly, in the case of the Na^+−CE complex, the selectivities (i.e., 4.571, 4.877, and 4.947) were larger than the other complexed metal ions. The selectivity sequence of the complexed metal ions is known to depend on the metal ion size and the ligand cavities.[15] The high selectivity of the complexed metal ion signifies the good extraction ability of CE for metal ions in the nitrobenzene−water binary system.

2.2. MD Simulations. In this subsection, we will first report the phase separation of the nitrobenzene−water mixtures so as to understand the extraction mechanism. The following sections will then demonstrate the computation of binding energies, free energies, and the interaction energies of the complexed metal ions using the explicit and implicit solvent models.

2.2.1. Demixing Simulations for the Binary Nitrobenzene−Water Solution. In this section, phase separation of nitrobenzene−water binary mixtures containing the ionophore (DB18C6) and the salts (i.e., $Cs^+NO_3^-$, $K^+NO_3^-$, $Na^+NO_3^-$,

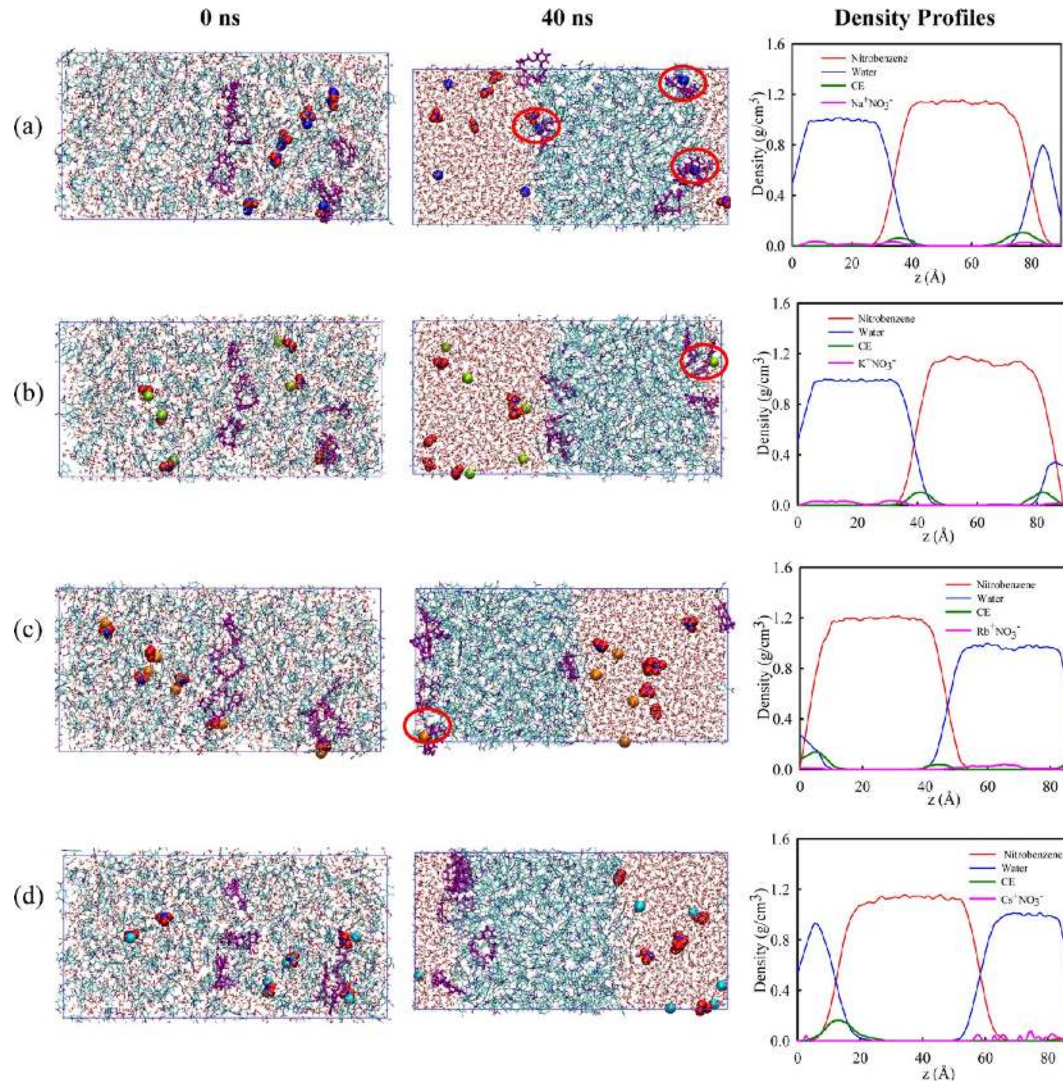

Figure 3. Initial and final snapshots of nitrobenzene−water demixing systems with (a) $Na^+NO_3^-$ (blue), (b) $K^+NO_3^-$ (yellow), (c) $Rb^+NO_3^-$ (orange), (d) $Cs^+NO_3^-$ (cyan), and DB18C6 at 1:1 (metal ion/ligand) ratio. Plots for density profiles of solvents and solutes for each system are given in the last column.

DOI: 10.1021/acsomega.7b01828
ACS Omega 2018, 3, 1663−1674

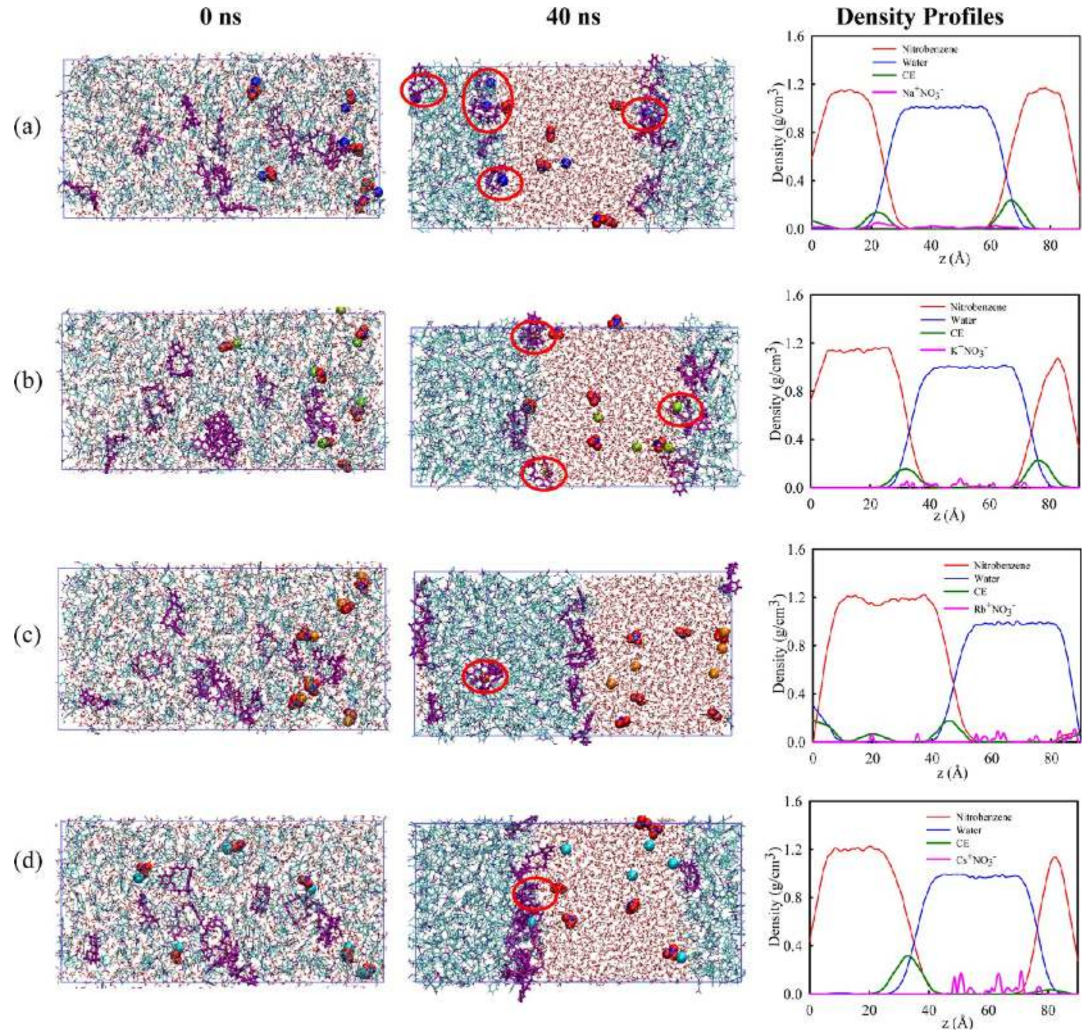

Figure 4. Initial and final snapshots of nitrobenzene−water demixing systems with (a) $Na^+NO_3^-$ (blue), (b) $K^+NO_3^-$ (yellow), (c) $Rb^+NO_3^-$ (orange), (d) $Cs^+NO_3^-$ (cyan), and DB18C6 at 1:2 (metal ion/ligand) ratio. Plots for density profiles of solvents and solutes for each system are given in the last column.

and $Rb^+NO_3^-$) is reported. The two liquids were found to be separated rapidly after 1 ns run, forming two clean bulk phases. During the dynamics, the hydrophilic moieties of the solutes (i.e., Cs^+, K^+, Na^+, and Rb^+) were found to diffuse from the bulk aqueous phase to the nitrobenzene side of the interface in the presence of ionophore. This is observed from the density curves of metal ions pointing to the broad peak near the interface at 40 ns (Figures 3−5). The MD simulations were carried out at four-metal ion to CE ligand (M/L) stoichiometric ratios: 1:1 (i.e., 6 M^+ and 6 DB18C6), 1:2 (i.e., 6 M^+ and 12 DB18C6), and 2:1 (i.e., 12 M^+ and 6 DB18C6). In the $Na^+NO_3^-$ (1:1) system, the first complexation of Na^+ with DB18C6 was observed only after 3 ns of simulation time, whereas at the end of the dynamics, we observed three complexes at the interface (Figure 3a). The position of the complexes is specified by red circles, as shown in Figure 3. In the case of $K^+NO_3^-$ (1:1) and $Rb^+NO_3^-$ (1:1) systems, the complexation was observed at 12 and 17 ns, respectively. Both the complexes were found to be located near the interface (Figure 3b,c). In the case of $Cs^+NO_3^-$ system, a single Cs^+ ion was found to diffuse from the bulk aqueous phase to the interface (Figure 3d).

In the 1:2 $Na^+NO_3^-$ system, the first complexation was observed at 1 ns, which slowly increased to five toward the end of simulation. However, all of the complexes were observed to appear at the interface (Figure 4a). The partitioning of Na^+ was increased with increasing CE ligand concentration. On the other hand, for the $K^+NO_3^-$ system, the complexation of K^+ with DB18C6 was observed at 5 ns, whereas at the end of the simulation, three complexes were placed at the interface, as indicated by the density profiles (Figure 4b). In the $RbNO_3$ system, the complexation of Rb^+ with DB18C6 was observed after 17 ns (Figure 4c) and in the $CsNO_3$ system, the complexation of Cs^+ with DB18C6 was observed at 23 ns at the interface (Figure 4d).

For the 2:1 $Na^+NO_3^-$ system, the first complexation of Na^+ with DB18C6 was observed after 7 ns, whereas the second one was observed at 18 ns (Figure 5a). Both the complexes were found to be located near the interface (Figure 5a). In the other systems (i.e., $K^+NO_3^-$, $Rb^+NO_3^-$, and $Cs^+NO_3^-$), the complexation of M^+ with DB18C6 was observed at the interface and the complexes were solvated by the nitrobenzene molecules (Figure 5b−d).

To understand the cation exchange phenomena, we considered different metal salts in the systems. The MD

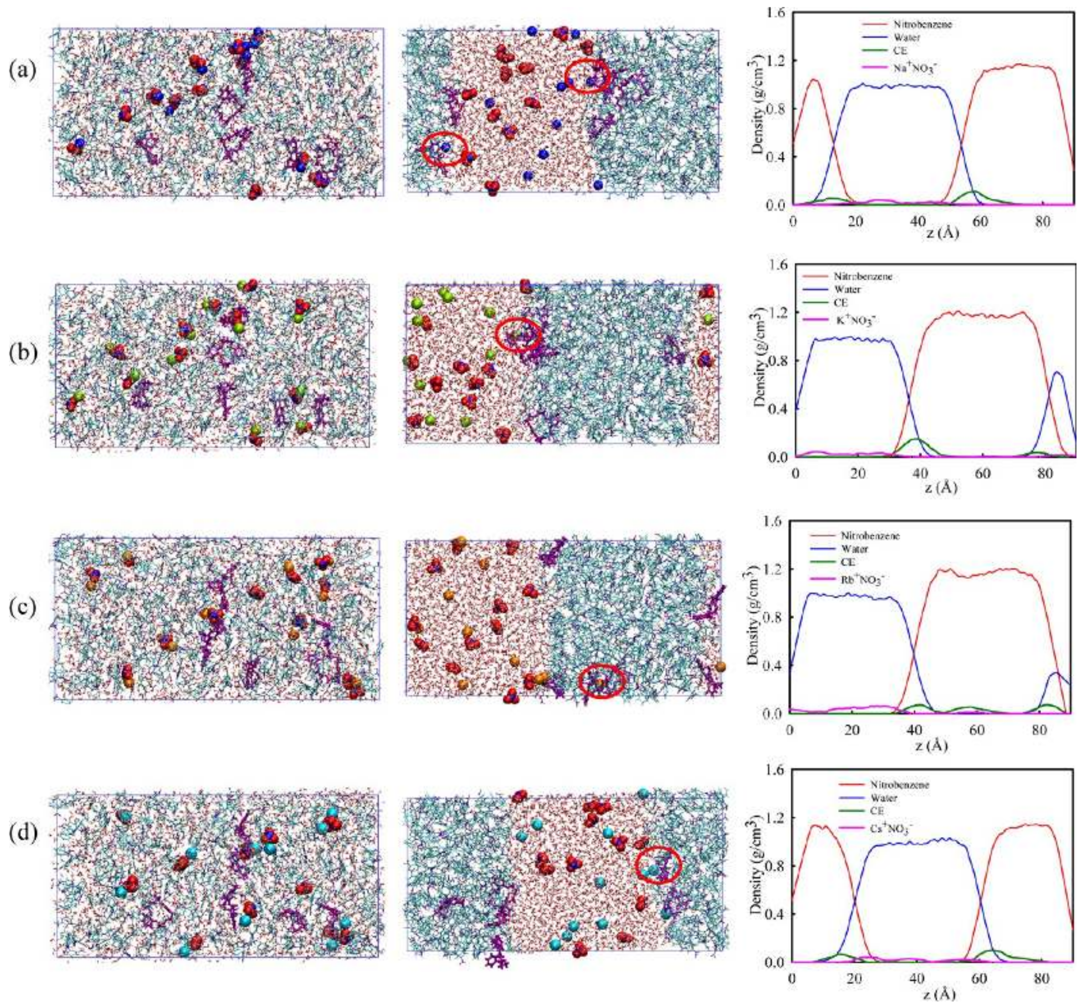

Figure 5. Initial and final snapshots of nitrobenzene−water demixing systems with (a) $Na^+NO_3^-$ (blue), (b) $K^+NO_3^-$ (yellow), (c) $Rb^+NO_3^-$ (orange), (d) $Cs^+NO_3^-$ (cyan), and DB18C6 at 2:1 (metal ion/ligand) ratio. Plots for density profiles of solvents and solutes for each system are given in the last column.

simulations were carried out with four metal salts (Na^+Cl^-, K^+Cl^-, $Rb_2{}^+SO_4{}^-$, and Cs^+Cl^-) and DB18C6 at the stoichiometric ratios of 1:1 (i.e., 6 M^+ and 6 DB18C6), 1:2 (i.e., 6 M^+ and 12 DB18C6), and 2:1 (i.e., 12 M^+ and 6 DB18C6) (Figures S1−S3, Supporting Information). We notice that the counter anions do not change the extraction behavior when compared to the same anion, that is, NO_3^- (Figures 3−5). Thus in all cases, Na^+ interacts more strongly with DB18C6 at the interface which can be derived from its higher stoichiometry. This also reflects in their experimental distribution coefficient in Table 2. It should be noted that the ionophore affects the extraction process by solvating the metal ion complex in the nitrobenzene phase which tends to depend on its dielectric constant, dipole moment, and the H-bonding ability. The results indicate that the smallest ion Na^+ is intrinsically preferred,[16] and it agrees with the large value of selectivity (4.947) as predicted by COSMO-RS (Table 1).

With respect to phase separation in $Cs^+NO_3^-$- and $Rb^+NO_3^-$-based systems [Figure 6a,b], the demixing index λ decreases down to 0.4 after 6.82 and 4.81 ns, respectively. One the other hand, when $K^+NO_3^-$ and $Na^+NO_3^-$ [Figure 6c,d] is represented as solutes in the system, λ decreases down to 0.4 in only 2.04 and 2.93 ns, respectively. Thus, it implies that an interface formation is faster for K^+- and Na^+-based systems when compared to Cs^+ and Rb^+ systems. The phase separation was found to be slower for the $Cs^+NO_3^-$-based system. This is expected as the solvation phenomena are known to be stronger in the cesium-based system owing to its higher concentration of charge. Although all systems demix readily, the outcome of phase separation depends on the nature and concentration of the solute.[17] In all of the profiles, λ decreases from 0.9 (mixed state) and approaches an equilibrium value of 0.4 (separated phases) to well-separated phases at 40 ns. The final value is not exactly zero because the densities of the liquids overlap in the interfacial region.[17]

Table 2. Experimental Distribution Coefficients of the Metal Ions in the Organic Phase in the Presence of CEs (0.1 M DB18C6)

metal ion	D_{Exp} (1:1)	D_{Exp} (1:10)	D_{Exp} (10:1)
Cs^+	0.001	0.010	0.024
Rb^+	0.001	0.020	0.025
K^+	0.028	0.055	0.042
Na^+	0.059	0.060	0.056

2.2.2. Structural Properties of Metal Ions in the Nitrobenzene−Water Demixing System. The structure of the solvent molecules around the alkali metal ions is usually

DOI: 10.1021/acsomega.7b01828
ACS Omega 2018, 3, 1663−1674

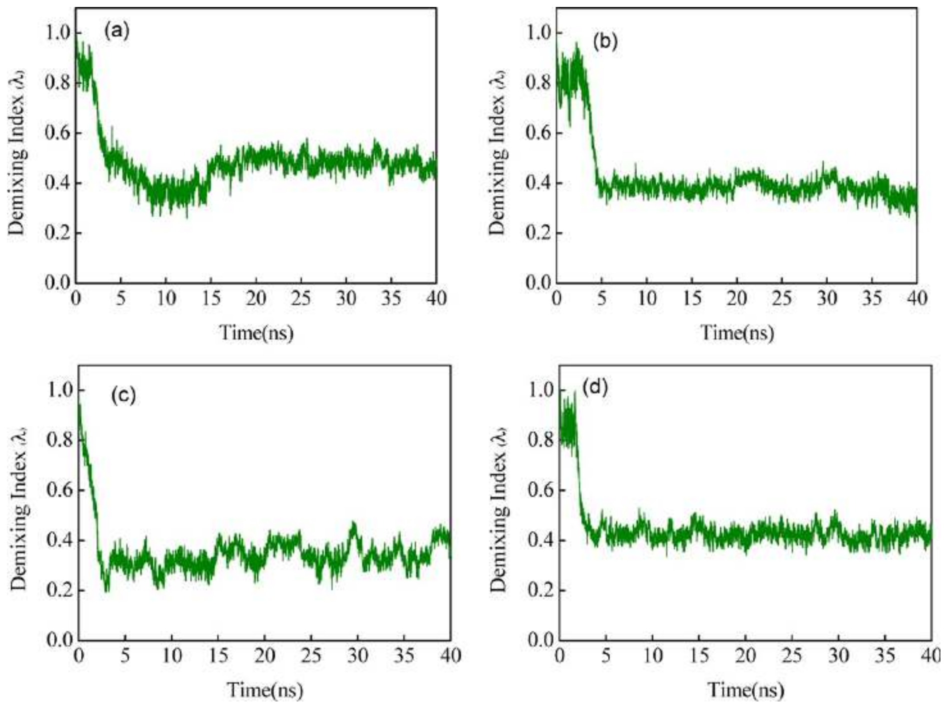

Figure 6. Variation of demixing index (λ) with time in the nitrobenzene−water system with different metal ions and DB18C6: (a) $Cs^+NO_3^-$, (b) $Rb^+NO_3^-$, (c) $K^+NO_3^-$, and (d) $Na^+NO_3^-$.

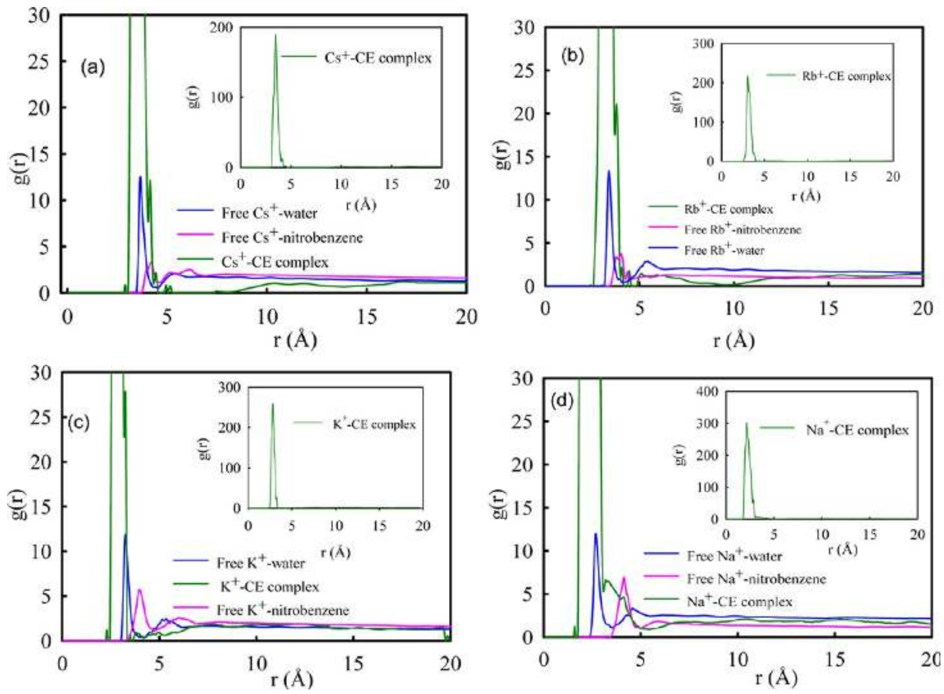

Figure 7. RDFs for (a) Cs^+−CE complex (green), free Cs^+−water (blue), and free Cs^+−nitrobenzene (pink), (b) free Rb^+−CE (green), free Rb^+−water (blue), and free Rb^+−nitrobenzene (pink), (c) free K^+−CE (green), free K^+−water (blue), and free K^+−nitrobenzene (pink), and (d) free Na^+−CE (green), free Na^+−water (blue), and free Na^+−nitrobenzene (pink).

obtained by the RDFs. The RDF plots of the metal ions (i.e., Cs^+, K^+, Na^+, and Rb^+) with the oxygen atoms of CE, nitrobenzene, and water are depicted in Figure 7. A sharp peak in the RDF of the Cs^+−CE complex at 3.25 Å (Figure 7a) indicates the formation of the complex. The pair correlation function $g(r)$ corresponds to the interaction between the metal ion and the center of mass of DB18C6 CE. A sharp peak in the RDF of the Cs^+−CE complex at 3.45 Å (Figure 7a) indicates the formation of the complex. Similarly, sharp peaks of large magnitude between the metal ions and the oxygen atom of DB18C6 were obtained at 3.05 (Rb^+), 2.85 (K^+), and 2.23 Å (Na^+). Hence, it can be observed that the position of the sharp peaks changes monotonously with decreasing the ion size from Cs^+ to Na^+. This indicates the formation of a highly stable complex (Figure 7a−d) for all of the metal ions. Similar large peaks between the metal ions and the oxygen atom of water

DOI: 10.1021/acsomega.7b01828
ACS Omega 2018, 3, 1663−1674

were obtained at 2.65 (Na^+), 3.25 (K^+), 3.35 (Rb^+), and 3.65 Å (Cs^+) (Figure 7). This suggests a reasonably strong association of the metal ions with water as compared to that with nitrobenzene. In addition, it was observed that the nitrobenzene molecules formed a well-defined first solvation shell around the metal ions but a weaker second solvation shell. This indicates that long-range ordering of the complex was not possible. The coordination number of the nitrobenzene molecules in the first solvation shell of the metal ion was obtained by integrating the M^+−O (nitrobenzene) RDFs till the first minimum. The results are given in Table 3. The

Table 3. Coordination Numbers of the First Solvation Shell for Metal Ions in Different Systems Obtained from the MD Simulations

simulated system	water	nitrobenzene	crown ether
$Cs^+NO_3^-$	35.67	1.54	1.37
$Rb^+NO_3^-$	27.92	1.74	1.28
$K^+NO_3^-$	25.84	2.96	2.31
$Na^+NO_3^-$	12.91	4.15	3.17

coordination numbers (Table 3) of free Cs^+, K^+, and Rb^+ (i.e., 35.67, 25.84, and 27.92) were much larger than that of Na^+ within the first solvation shell. This is due to the fact that higher fractions of Cs^+, K^+, and Rb^+ were coordinated with the oxygen atoms of water. The Na^+ ion was found to be surrounded by three to four oxygen atoms of CE. The higher coordination number of Na^+ (i.e., 3.17) than the other metal ions (i.e., K^+, Cs^+, and Rb^+) suggests the formation of complexes with high stability.

Figure 8 represents the spatial distribution functions (SDFs) that provide the average density of different metal ions around a reference CE, water, and a nitrobenzene molecule. These SDFs are obtained using TRAVIS package.[18] The isovalue employed for the SDFs corresponding to the metal ion−CE is 3.5 particle Å, whereas for the metal ion−nitrobenzene and metal ion−water, the isovalues are 0.05 and 0.02 particle Å, respectively. As can be seen, the more active ("O atom") side of CE is surrounded by Na^+ ion, whereas the less active side of CE surrounds the Cs^+ ion. Moreover, the appearance of the distribution of the Na^+ ion around the active side of nitrobenzene is closer than that of other metal ions. This finding is in accordance with the RDF plots involving Na^+−CE and Na^+−nitrobenzene (Figure 7). In specific, the positions of the first peak of these RDFs appear at 2.23 and 4.16 Å, respectively. Furthermore, Na^+ ions are distributed at a distance that is very far from the water molecule. Therefore, other metal ions (i.e., Cs^+, Rb^+, and K^+) are very closely distributed around the active sides of the water molecule.

2.3. Explicit and Implicit Solvent Models. The binding, interaction, and free energies with the solvents for free metal ions and the complexes are computed using both explicit solvent as well as PCM approach. Figure 9 shows the schematic diagram for calculating the binding and interaction energies in vacuo using explicit and implicit solvents. Binding energies of the complexed metal ions in vacuo were calculated by eq 2[19]

$$\Delta E^0 = \Delta E^0_{\mathrm{Cs-CE}} - (\Delta E^0_{\mathrm{Cs}} + \Delta E^0_{\mathrm{CE}}) \tag{2}$$

where $\Delta E^0_{\mathrm{Cs-CE}}$, ΔE^0_{Cs}, and ΔE^0_{CE} are the energies of the complex, metal ion, and CE, respectively, in vacuo. Here, the values of the binding energies in vacuo were defined based on a thermodynamic cycle. Interaction energies, $\Delta E_Z^{\mathrm{int}(N)}$, were

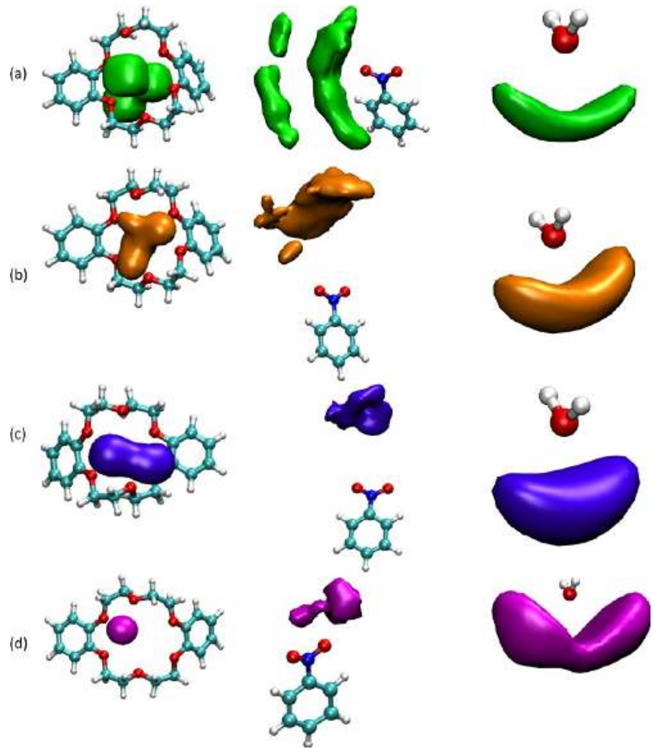

Figure 8. SDFs of the IL−water binary mixed system. (a) Na^+ ion around CE, nitrobenzene, and water, (b) K^+ ion around CE, nitrobenzene, and water, (c) Rb^+ ion around CE, nitrobenzene, and water, and (d) Cs^+ ion around CE, nitrobenzene, and water.

calculated between the solute Z and the solvent molecules N as per eq 3.

$$\Delta E_Z^{\mathrm{int}(N)} = \Delta E_Z{}^N - (\Delta E_Z^0 + \Delta E_{\mathrm{solv\text{-}Z}}) \tag{3}$$

The superscript, N, represents the number of solvent molecules, and 0 indicates their absence. ΔE_Z^0 and $\Delta E_{\mathrm{solv\text{-}Z}}$ represent the energy of the solute in vacuo and the energy of the N solvent molecules in the geometry of the system (i.e., Z + solvent), respectively. The calculated binding and free energies of the free and the complexed metal ions are depicted in Figure 10. From Figure 10a,b, it is clear that the binding and free energies of Na^+ (i.e., −163.07 and −162.09 kcal/mol) were higher than the same for the other free metal ions (i.e., Cs^+, K^+, and Rb^+) in vacuo. The calculated binding and free energies for Na^+ with CE (i.e., −78.41 and −68.06 kcal/mol, respectively) were also found to be higher than those of the other complexed metal ions (Figure 10c,d). The binding energy for Na^+ with DB18C6 using SDD basis set was higher than those of the other ions, indicating a higher selectivity of Na^+ over the other metal ions. The binding and free energies for the free and complexed metal ions in vacuo follow the sequence of selectivity obtained from COSMO-RS, that is, $Na^+ > K^+ > Rb^+ > Cs^+$.

A comparison between the values of interaction energies obtained from the explicit solvent model and the PCM is presented in Table 4. The interaction energies between the solute and the solvent molecules were calculated by using the difference between the energies obtained in the PCM solvent and the same in vacuo. The binding energies in the implicit solvent model were calculated from the energies in the PCM solvent. The binding energy of the complexed metal ions in the implicit solvent model was calculated from eq 4.

DOI: 10.1021/acsomega.7b01828
ACS Omega 2018, 3, 1663−1674

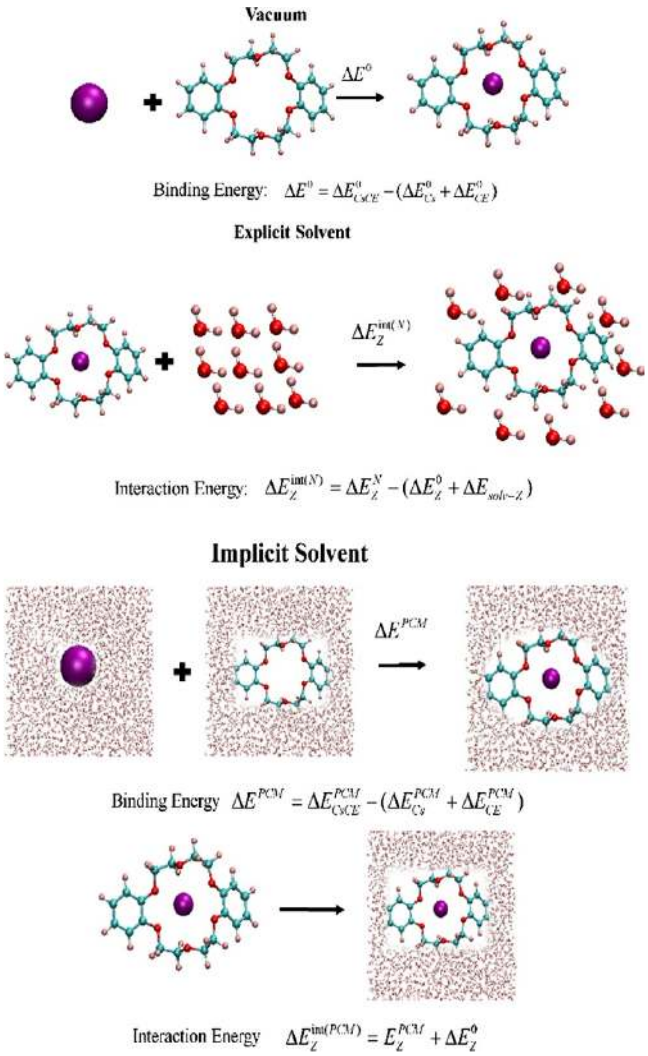

Figure 9. Schematic diagram of the computational procedure used to calculate binding and interaction energies in vacuo: explicit and implicit solvent based on structures obtained from QC calculations.

$$\Delta E^{PCM} = \Delta E^{PCM}_{CsCE} - (\Delta E^{PCM}_{Cs} + \Delta E^{PCM}_{CE}) \quad (4)$$

The calculated binding energies for metal ions with CE in PCM solvents (i.e., water and nitrobenzene) are presented in Figure 11. The calculated binding energies of the Na^+−CE complex in water (i.e., −67.87 kcal/mol) and nitrobenzene (i.e., −151.03 kcal/mol) were found to be higher than those of the other complexed metal ions. The binding energies of K^+−CE and Rb^+−CE complexes (i.e., −54.96 and −55.94 kcal/mol, respectively) in nitrobenzene and water were quite similar (Figure 11a). On the other hand, the calculated binding energies of Cs^+ and Rb^+ (i.e., −132.61 and −137.14 kcal/mol, respectively) with CE were quite close in nitrobenzene (Figure 11b).

The calculated interaction energies obtained from the MD simulations and the different solvent models are summarized in Table 4. The implicit solvent model reduces the stabilization of the complex in water as compared to the interaction energy in the explicit model (Table 4). The reduction of the implicit solvent model mainly depends on the dielectric permittivity of the medium. In both the solvent models, the interaction energy (ΔE) between the Na^+−CE complex and nitrobenzene was found to be higher (i.e., −289.92 and −143.12 kcal/mol) than those of the other metal ions (i.e., Cs^+, K^+, and Rb^+), indicating the higher selectivity for Na^+ over the other metal ions. From the results reported in Table 4, it is clear that the smallest ion Na^+ is intrinsically preferred, in the order: $Na^+ > K^+ > Rb^+ > Cs^+$. Hence, the results obtained from the MD simulations and the explicit and implicit solvation models on the preferential selectivity of Na^+ over other competing metal ions with DB18C6 exactly agree with the selectivities predicted by COSMO-RS.

Overall, we have used MD combined with quantum mechanics (QM) to calculate the interaction energies of the complex with the solvents. We have compared the predictions of explicit and implicit solvation models and have related them to the structures observed in MD trajectories. The optimized potential for liquid simulation force field, which includes the bonded, van der Waals, and electrostatic interactions, is used in MD to calculate interaction energies, whereas QM calculations are based on all-electron ab initio approach. Results were averaged over about 1000 structures (last 5 ns of the MD trajectory). Interaction energies of the complex with solvents observed in MD differ with the predictions of the QM model. We suggest that this discrepancy results from the structure of the complex used in explicit solvent calculations at the optimal geometry, whereas the coordination of the complex with solvent molecules as observed from simulations is different. Further, the PCM interaction energies depend on the dielectric permittivity of the medium and polarity of the liquid. We conclude that the differences between MD simulations and the predictions of the QM model can be attributed to the structure of the studied systems as well as the fundamental level of approach is different.

3. CONCLUSIONS

This paper reports experimental studies combined with COSMO-RS and molecular dynamics (MD) simulations to study the intermolecular interactions between the solute and the solvent (i.e., nitrobenzene and water). A comparison has been made between the interaction energies computed using both explicit and implicit solvent models. The sigma profiles of the metal ions and their complexes were used to understand the miscibility of the components. From the experimental data, it has been shown that the distribution constant of the Na^+ ion is found to be higher than those of the other metal ions in the nitrobenzene−water binary mixture, which is in good agreement with the COSMO-RS predictions at three different temperatures. The calculated interaction energies for the Na^+−CE complex with nitrobenzene obtained by MD and QC were also found to be higher than those for other metal ion complexes. While on one end, COMSO-RS gave a qualitative aspect for the distribution coefficient, on the other end, the experimental and MD- or QC-predicted interaction energies validated the COSMO-RS phenomena. The selectivities of the metal ions predicted by COSMO-RS decreased with increasing metal ion size in the sequence: $Na^+ > K^+ > Rb^+ > Cs^+$. The higher binding and interaction energies for the Na^+−CE complex indicated the higher selectivity of Na^+ over the other metal ions, which complemented well with the COSMO-RS predictions.

4. COMPUTATIONAL DETAILS

4.1. COSMO-RS Model. The COSMO-RS method has been extensively used to predict thermodynamic properties of

DOI: 10.1021/acsomega.7b01828
ACS Omega 2018, 3, 1663−1674

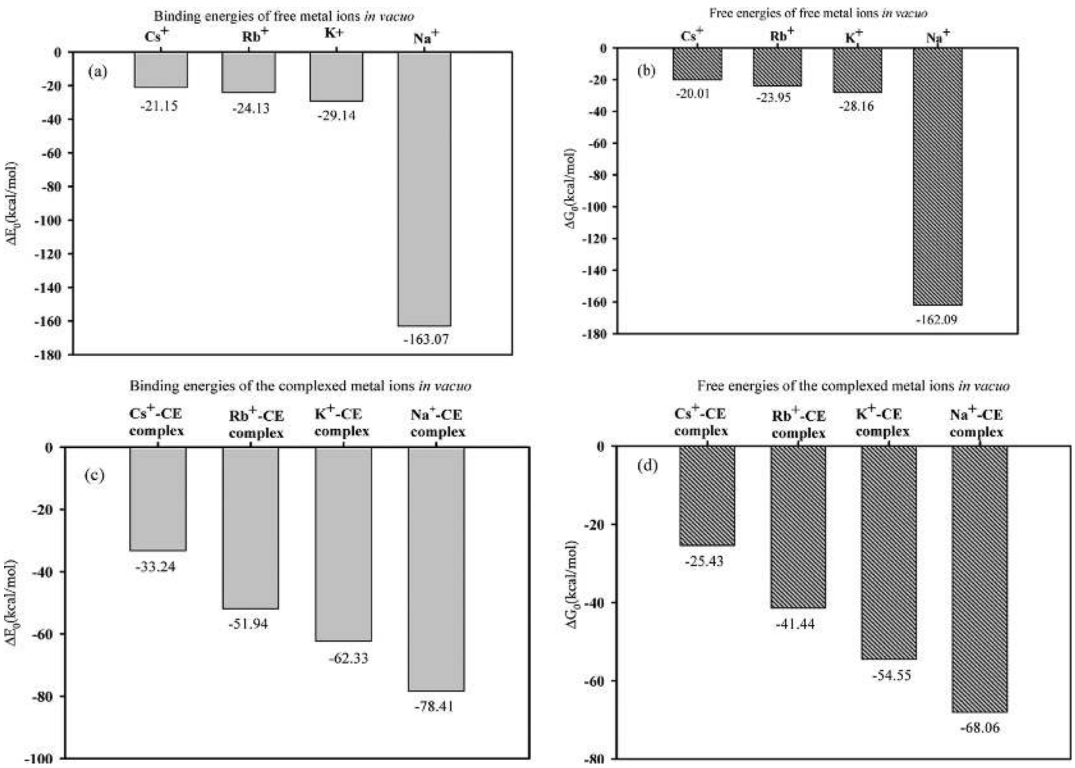

Figure 10. Binding energies and free energies (in kcal/mol) for free metal ions (a,b) and complexed metal ions (c,d) obtained from QC calculations.

Table 4. Interaction Energies (kcal/mol) of the Complex with the Solvent Calculated by QC and MD Simulation

	ΔE_{MD}		$\Delta E_{Explicit}$		ΔE_{PCM}	
species	water	nitrobenzene	water	nitrobenzene	water	nitrobenzene
Cs^+−CE complex	−97.87	−128.71	−77.94	−121.79	−50.48	−130.14
Rb^+−CE complex	−85.28	−164.92	−87.34	−152.45	−51.33	−133.76
K^+−CE complex	−78.51	−211.56	−89.71	−198.62	−55.99	−140.83
Na^+−CE complex	−56.86	−271.65	−92.39	−289.92	−56.69	−143.12

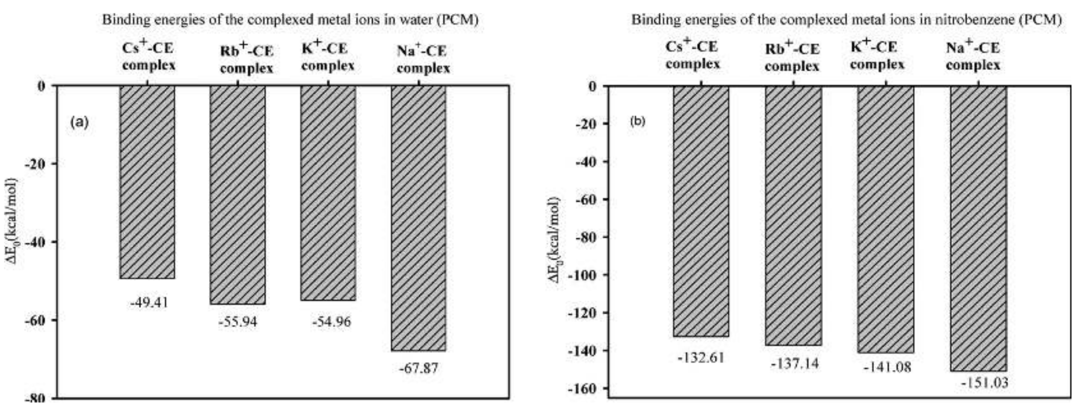

Figure 11. Binding energies (in kcal/mol) for complexed metal ions in (a) water and (b) nitrobenzene (PCM approach) obtained from QC calculations.

fluids and liquid mixtures. The COSMO-RS method was first reported by Klamt[11] and co-workers.[10,20] In the COSMO-RS model, the interactions of the molecular surfaces are determined by an interaction energy function, which depends on the screening charge densities. The screening charges are developed when the solute is placed in the midst of a conductor. The screening charges so produced are unique for each solute, and they are depicted in the form of histogram or probabilistic distributions. This probability distribution is estimated by the sigma profile[11]

$$P(\sigma) = A_i(\sigma)/A_i \quad (5)$$

Here, $A_i(\sigma)$ is the total surface area of the segment with a charge density σ, and A_i is the total surface area of the entire solute. The activity coefficient of a molecule is then obtained by reducing the information for predicting segment potential using

DOI: 10.1021/acsomega.7b01828
ACS Omega 2018, 3, 1663−1674

a statistical mechanical framework. The global adjustable parameters such as the surface area of the segment (a_{eff} = 6.32 Å^2), the hydrogen-bonding interaction constant (c_{HB} = 75 006 kcal A^4/(mol e^2)), and the cutoff for hydrogen-bonding interaction (σ_{HB} = 0.0084 e/Å^2) are then subsequently used for the activity coefficient predictions.[21] In this work, the initial COSMO files were generated by the BVP86/TZVP/DFT level of theory.[22] These files contain the screening charge densities of the molecule concerned. These screening charges are then clubbed together in the form of sigma profile which is probabilistic in nature (eq 5). The information within the sigma profile is then used to compute the activity coefficient using a statistical thermodynamic framework (RS).[10−14] The equations and methodology are available in our earlier reported prediction on the COSMO-RS model.[14] All of the calculations were performed with the Gaussian 09 package.

4.2. Quantum Calculation. The structures of all molecules were drawn using the molecule visualization and editing program Gauss View 5.0, whereas the geometry was optimized by B3LYP in Gaussian 09 package. The frequency was estimated by using the *freq* command by B3LYP/SDD/DFT level of theory.[23] The individual solutes in the implicit solvent model (PCM) were optimized with the same functional theory and SDD(+) basis.[23] The single-point energy calculations were carried out at the MP2/SDD(+)/PCM level.

4.3. Molecular Dynamics. The MD simulations were performed by NAMD,[24] version 2.9, where the potential energy is given by

$$U = \sum_{ij}^{\text{bonds}} \frac{k_{r,ij}}{2}(r_{ij} - r_{0,ij})^2 + \sum_{ijk}^{\text{angles}} \frac{k_{\theta,ijk}}{2}(\theta_{ijk} - \theta_{0,ijk})^2 + \sum_{ijkl}^{\text{dihedrals}} \sum_{m=1}^{4} \frac{v_{m,ijkl}}{2}[1 + (-1)^m \cos(m\varphi_{ijkl})] + \sum_i \sum_{j\neq i}' \left\{ 4\varepsilon_{ij}\left[\left(\frac{\sigma_{ij}}{r_{ij}}\right)^{12} - \left(\frac{\sigma_{ij}}{r_{ij}}\right)^{6}\right] + \frac{1}{4\pi\varepsilon_0}\frac{q_i q_j}{r_{ij}} \right\} \tag{6}$$

The first three terms denote the sum of bond, angle, and dihedral energies. The last term corresponds to the sum of electrostatic and van der Waals interactions between the nonbonded atoms. The parameters for nitrobenzene were taken from an earlier work.[25,26] The parameters for metal ions (i.e., Cs^+, K^+, Na^+, and Rb^+) were reported by Joung and Cheatham,[27] whereas the same for the nitrate ion was obtained from Lopes et al.[28] We have used the TIP3P model[29] for water. The force field parameter for DB18C6 was taken from Sahu et al.[30] and Weiner et al.[31] The atomic charges were regressed by the CHELPG method,[32] whereas the nonbonded interactions were calculated using a 12 Å atom-based cutoff. The solutions were represented with three-dimensional periodic boundary conditions, whereby alternating slabs of water and nitrobenzene are observed in the case of biphasic systems.[33]

The MD simulations were performed at 300 K in the (NVT) ensemble. The temperature and pressure were controlled by Langevin thermostat and Langevin piston, respectively. The simulated systems are provided in Table 5. The systems were subjected to 10 000 steps of energy minimization followed by equilibration in NPT ensemble at 300 K and 1 atm. The total time of the simulation was kept at 2 ns. All of the bond lengths were constrained by SHAKE, and the Verlet algorithm was used to integrate the equations of motion. Snapshots for the trajectory were taken from VMD software.[34] The densities of nitrobenzene (ρ_{ni}) and water (ρ_w) were plotted as a function of the z-coordinate. The phase separation as a function of time was described by the demixing index (λ). This value ranges from 1 (for a perfectly mixed system) to 0 (for completely separated phases).

Table 5. Size of the Simulation Boxes and the Number of Molecules at 300 K

systems	solutes	box size x, y, z (Å^3)	time (ns)
nitrobenzene−water (demixing)	6 $Cs^+NO_3^-$; 6 DB18C6	43.22 × 43.22 × 86.44	40
nitrobenzene−water (demixing)	6 $Cs^+NO_3^-$; 12 DB18C6	43.36 × 43.36 × 86.72	40
nitrobenzene−water (demixing)	12 $Cs^+NO_3^-$; 6 DB18C6	43.24 × 43.24 × 86.48	40
nitrobenzene−water (demixing)	6 $K^+NO_3^-$; 6 DB18C6	42.74 × 42.74 × 85.49	40
nitrobenzene−water (demixing)	6 $K^+NO_3^-$; 12 DB18C6	42.98 × 42.98 × 85.97	40
nitrobenzene−water (demixing)	12 $K^+NO_3^-$; 6 DB18C6	42.79 × 42.79 × 85.58	40
nitrobenzene−water (demixing)	6 $Na^+NO_3^-$; 6 DB18C6	43.18 × 43.18 × 86.36	40
nitrobenzene−water (preinterface)	6 $Na^+NO_3^-$; 12 DB18C6	43.52 × 43.52 × 87.05	40
nitrobenzene−water (demixing)	12 $Na^+NO_3^-$; 6 DB18C6	43.11 × 43.11 × 86.23	40
nitrobenzene−water (demixing)	6 $Rb^+NO_3^-$; 6 DB18C6	42.80 × 42.80 × 85.60	40
nitrobenzene−water (preinterface)	6 $Rb^+NO_3^-$; 12 DB18C6	43.01 × 43.01 × 86.02	40
nitrobenzene−water (preinterface)	12 $Rb^+NO_3^-$; 6 DB18C6	42.78 × 42.78 × 85.57	40

$$\frac{1}{\lambda} = \frac{1}{N}\left(\frac{1}{\rho_w} + \frac{1}{\rho_{ni}}\right) \tag{7}$$

Here, N is the normalization factor.

5. EXPERIMENTS FOR DETERMINING METAL ION DISTRIBUTION

5.1. Reagents and Solutions. DB18C6, >98% assay, was purchased from Alfa Aesar. DB18C6 solution (0.1 M) in nitrobenzene (AR grade, SDFine make) was prepared by dissolving 3.604 g of CE in 100 mL of nitrobenzene. Analytical-grade sodium chloride (Chemco Fine Chemicals), potassium chloride (Thomas Baker), rubidium sulfate (Merck), and cesium chloride (Sisco Research Laboratories Pvt. Ltd.) were used for preparing 0.1 M of individual alkali metal ion (Na/K/Rb/Cs) solution by dissolving an appropriate amount of the above alkali metal salts in acidified water. Millipore water (a resistivity of 18.2 mΩ·cm) was used in all experiments.

5.2. Solvent Extraction Studies. The organic phase was prepared by diluting 0.1 M DB18C6 to 0.01 M DB18C6 in nitrobenzene. The 0.1 M alkali metal ion solution was used as the aqueous phase. Each 5 mL of the aqueous and the organic phases was stirred at 800 rpm using a multiposition stirrer (make: IKA, model: RT 10 POWER MAG). Then, the solution mixture was allowed to stand for 30 min until the phases clearly separated. The extraction experiments were carried out at four-metal to CE ligand mole ratios: 10:1 (i.e., 0.1 M M^+ and 0.01 M DB18C6), 1:1 (i.e., 0.01 M M^+ and 0.01 M DB18C6), and 1:10 (i.e., 0.001 M M^+ and 0.01 M DB18C6). The distribution coefficient was determined by comparing the metal ion

DOI: 10.1021/acsomega.7b01828
ACS Omega 2018, 3, 1663−1674

concentrations in the aqueous phases before and after extraction. An inductively coupled plasma mass spectrometry, developed at TPD, Bhabha Atomic Research Centre (Mumbai, India), was employed to estimate the alkali metal ion concentration in the aqueous phase after appropriate dilution. Equation 8 was used for calculating the distribution coefficient (D).

$$D = \frac{C_{org}}{C_{aq}} = \left(\frac{C_o - C_e}{C_e}\right)\left(\frac{V_{aq}}{V_{org}}\right) \tag{8}$$

where C_{org} and C_{aq} are the concentrations of the extracted alkali metal ion in the organic phase and the retained alkali metal ion in the aqueous phase, respectively. C_o and C_e are the initial and final concentrations of the alkali metal ion in the aqueous phase, respectively. V_{aq} is the volume of the aqueous phase, and V_{org} is the volume of the organic phase. The values of D for DB18C6 are reported in Table 2.

■ ASSOCIATED CONTENT

Supporting Information

The Supporting Information is available free of charge on the ACS Publications website at DOI: 10.1021/acsomega.7b01828.

Initial and final snapshots of nitrobenzene−water demixing systems (PDF)

■ AUTHOR INFORMATION

Corresponding Author

*E-mail: tamalb@iitg.ernet.in (T.B.).

ORCID

Tamal Banerjee: 0000-0001-8624-6586

Sk. Musharaf Ali: 0000-0003-0457-0580

Notes

The authors declare no competing financial interest.

■ ACKNOWLEDGMENTS

This work was funded by the Board of Research in Nuclear Sciences (BRNS, Government of India) vide scheme no. 2013/36/30-BRNS/2352, dated 26.11.2013.

■ REFERENCES

(1) Bonnesen, P. V.; Delmau, L. H.; Moyer, B. A.; Lumetta, G. J. Development of effective solvent modifiers for the solvent extraction of cesium from alkaline high-level tank waste. *Solvent Extr. Ion Exch.* **2003**, *21*, 141−170.

(2) Herbst, R. S.; Law, J. D.; Todd, T. A.; Romanovskiy, V. N.; Babain, V. A.; Esimantovskiy, V. M.; Smirnov, I. V.; Zaitsev, B. N. Universal solvent extraction (UNEX) flowsheet testing for the removal of cesium, strontium, and actinide elements from radioactive, acidic dissolved calcine waste. *Solvent Extr. Ion Exch.* **2002**, *20*, 429−445.

(3) Gutsche, C. D.; Dhawan, B.; No, K. H.; Muthukrishnan, R. Calixarenes. 4. The synthesis, characterization, and properties of the calixarenes from p-tert-butylphenol. *J. Am. Chem. Soc.* **1981**, *103*, 3782−3792.

(4) Luo, H.; Dai, S.; Bonnesen, P. V.; Buchanan, A. C.; Holbrey, J. D.; Bridges, N. J.; Rogers, R. D. Extraction of cesium ions from aqueous solutions using calix [4] arene-bis (tert-octylbenzo-crown-6) in ionic liquids. *Anal. Chem.* **2004**, *76*, 3078−3083.

(5) McDowell, W. J.; Case, G. N.; McDonough, J. A.; Bartsch, R. A. Selective extraction of cesium from acidic nitrate solutions with didodecylnaphthalenesulfonic acid synergized with bis (tert-butylbenzo)-21-crown-7. *Anal. Chem.* **1992**, *64*, 3013−3017.

(6) Makrlík, E.; Hálová, J.; Kyrš, M. Contribution to the thermodynamics of complexes of alkali metal cations with dibenzo-18-crown-6 in water−nitrobenzene extraction system. *Collect. Czech. Chem. Commun.* **1984**, *49*, 39−44.

(7) Michael, D.; Benjamin, I. Molecular dynamics simulation of the water|nitrobenzene interface. *J. Electroanal. Chem.* **1998**, *450*, 335−345.

(8) Jorge, M.; Cordeiro, M. N. D. S. Intrinsic Structure and Dynamics of the Water/Nitrobenzene Interface. *J. Phys. Chem. C* **2007**, *111*, 17612−17626.

(9) dos Santos, D. J. V. A.; Gomes, J. A. N. F. Molecular dynamics study of the calcium ion transfer across the water/nitrobenzene interface. *ChemPhysChem* **2002**, *3*, 946−951.

(10) Klamt, A.; Schüürmann, G. COSMO: a new approach to dielectric screening in solvents with explicit expressions for the screening energy and its gradient. *J. Chem. Soc., Perkin Trans. 2* **1993**, 799−805.

(11) Klamt, A. Conductor-like screening model for real solvents: a new approach to the quantitative calculation of solvation phenomena. *J. Phys. Chem.* **1995**, *99*, 2224−2235.

(12) Lin, S.-T.; Sandler, S. I. A priori phase equilibrium prediction from a segment contribution solvation model. *Ind. Eng. Chem. Res.* **2002**, *41*, 899−913.

(13) Vishnoi, A.; Banerjee, T.; Ghosh, P.; Ali, S. M.; Shenoy, K. T. Theoretical prediction of distribution coefficients of Sr^{2+} in nuclear waste/ionic liquid phases using COSMO-RS model. *Sep. Purif. Technol.* **2014**, *133*, 138−148.

(14) Pilli, S. R.; Banerjee, T.; Mohanty, K. Extraction of pentachlorophenol and dichlorodiphenyltrichloroethane from aqueous solutions using ionic liquids. *J. Ind. Eng. Chem.* **2012**, *18*, 1983−1996.

(15) Katsuta, S.; Ito, Y.; Takeda, Y. Stabilities in nitromethane of alkali metal ion complexes with dibenzo-18-crown-6 and dibenzo-24-crown-8 and their transfer from nitromethane to other polar solvents. *Inorg. Chim. Acta* **2004**, *357*, 541−547.

(16) Wipff, G.; Lauterbach, M. Complexation of alkali cations by calix [4] crown ionophores: conformation and solvent dependent Na^+/Cs^+ binding selectivity and extraction: MD simulations in the gas phase, in water and at the chloroform-water interface. *Supramol. Chem.* **1995**, *6*, 187−207.

(17) Muzet, N.; Engler, E.; Wipff, G. Demixing of Binary Water−Chloroform Mixtures Containing Ionophoric Solutes and Ion Recognition at a Liquid−Liquid Interface: A Molecular Dynamics Study. *J. Phys. Chem. B* **1998**, *102*, 10772−10788.

(18) Brehm, M.; Kirchner, B. *TRAVIS—A Free Analyzer and Visualizer for Monte Carlo and Molecular Dynamics Trajectories*; ACS Publications, 2011.

(19) Eilmes, A.; Kubisiak, P. Li^+−Oligoglyme Association in the Presence of Ionic Liquid Studied by Molecular Dynamics and Explicit or Implicit Solvent Model. *J. Phys. Chem. B* **2015**, *119*, 11708−11720.

(20) Klamt, A.; Jonas, V.; Bürger, T.; Lohrenz, J. C. W. Refinement and parametrization of COSMO-RS. *J. Phys. Chem. A* **1998**, *102*, 5074−5085.

(21) Banerjee, T.; Anantharaj, R. *Desulphurization and Denitrification of Diesel Oil Using Ionic Liquids*; Elsevier: MA, USA, 2015; ISBN: 978-0-12-801347-2.

(22) Diedenhofen, M.; Klamt, A. COSMO-RS as a tool for property prediction of IL mixtures—a review. *Fluid Phase Equilib.* **2010**, *294*, 31−38.

(23) Bühl, M.; Sieffert, N.; Wipff, G. Density functional study of aqueous uranyl (VI) fluoride complexes. *Chem. Phys. Lett.* **2009**, *467*, 287−293.

(24) Kalé, L.; Skeel, R.; Bhandarkar, M.; Brunner, R.; Gursoy, A.; Krawetz, N.; Phillips, J.; Shinozaki, A.; Varadarajan, K.; Schulten, K. NAMD2: greater scalability for parallel molecular dynamics. *J. Comput. Phys.* **1999**, *151*, 283−312.

(25) Price, M. L. P.; Ostrovsky, D.; Jorgensen, W. L. Gas-phase and liquid-state properties of esters, nitriles, and nitro compounds with the OPLS-AA force field. *J. Comput. Chem.* **2001**, *22*, 1340−1352.

DOI: 10.1021/acsomega.7b01828
ACS Omega 2018, 3, 1663−1674

(26) Klauda, J. B.; Brooks, B. R. CHARMM force field parameters for nitroalkanes and nitroarenes. *J. Chem. Theory Comput.* **2008**, *4*, 107−115.
(27) Joung, I. S.; Cheatham, T. E., III Determination of alkali and halide monovalent ion parameters for use in explicitly solvated biomolecular simulations. *J. Phys. Chem. B* **2008**, *112*, 9020−9041.
(28) Canongia Lopes, J. N.; Deschamps, J.; Pádua, A. A. H. Modeling ionic liquids using a systematic all-atom force field. *J. Phys. Chem. B* **2004**, *108*, 2038−2047.
(29) Jorgensen, W. L.; Chandrasekhar, J.; Madura, J. D.; Impey, R. W.; Klein, M. L. Comparison of simple potential functions for simulating liquid water. *J. Chem. Phys.* **1983**, *79*, 926−935.
(30) Sahu, P.; Ali, S. M.; Singh, J. K. Structural and dynamical properties of Li^+-dibenzo-18-crown-6 (DB18C6) complex in pure solvents and at the aqueous-organic interface. *J. Mol. Model.* **2014**, *20*, 1−12.
(31) Weiner, S. J.; Kollman, P. A.; Nguyen, D. T.; Case, D. A. An all atom force field for simulations of proteins and nucleic acids. *J. Comput. Chem.* **1986**, *7*, 230−252.
(32) Breneman, C. M.; Wiberg, K. B. Determining atom-centered monopoles from molecular electrostatic potentials. The need for high sampling density in formamide conformational analysis. *J. Comput. Chem.* **1990**, *11*, 361−373.
(33) Sieffert, N.; Wipff, G. The [BMI][Tf2N] ionic liquid/water binary system: A molecular dynamics study of phase separation and of the liquid−liquid interface. *J. Phys. Chem. B* **2006**, *110*, 13076−13085.
(34) Humphrey, W.; Dalke, A.; Schulten, K. VMD: visual molecular dynamics. *J. Mol. Graphics* **1996**, *14*, 33−38.

DOI: 10.1021/acsomega.7b01828
ACS Omega 2018, 3, 1663−1674